Achieving ultrahigh carrier mobility and photo-responsivity in solution-processed perovskite/carbon nanotubes phototransistors

Hong Wang[1†], Feng Li[1†], Dominik Kufer[2], Weili Yu[1], Erkki Alarousu[3], Chun Ma[1], Yangyang Li[1], Zhixiong Liu[1], Changxu Liu[4], Nini Wei[5], Yin Chen[3], Fei Wang[6], Lang Chen[6], Omar F. Mohammed[3], Andrea Fratalocchi[4], Gerasimos Konstantatos[2], Tom Wu[1]*

[1]Materials Science and Engineering, King Abdullah University of Science and Technology, Thuwal 23955-6900, Kingdom of Saudi Arabia.

[2]ICFO- Institut de Ciencies Fotoniques, Mediterranean Technology Park, 08860 Castelldefels, Barcelona, Spain.

[3]Solar and Photovoltaics Engineering Research Center, King Abdullah University of Science and Technology, Thuwal 23955-6900, Kingdom of Saudi Arabia.

[4]PRIMALIGHT, Faculty of Electrical Engineering, Applied Mathematics and Computational Science, King Abdullah University of Science and Technology, Thuwal 23955-6900, Saudi Arabia.

[5]Core lab, King Abdullah University of Science and Technology, Thuwal 23955-6900, Kingdom of Saudi Arabia.

[6]Department of Electronic and Electrical Engineering, South University of Science and Technology of China, Shenzhen 518055, P.R. China.

[†]These authors contributed equally to this work.

*e-mail: tao.wu@kaust.edu.sa

Organolead trihalide perovskites have drawn substantial interest for applications in photovoltaic and optoelectronic devices due to their low processing cost and remarkable physical properties. However, perovskite thin films still suffer from low carrier mobility, limiting their device performance and application potential. Here we report that embedding single-walled carbon nanotubes into halide perovskite films can significantly enhance the hole and electron mobilities to record-high values of 595.3 and 108.7 $cm^2 V^{-1} s^{-1}$, respectively. In the ambipolar phototransistors with such hybrid channels, photo-carriers generated in the light-absorbing perovskite matrix are transported by the carbon nanotubes, leading to ultrahigh detectivity of 6×10^{14} Jones and responsivity of 1×10^4 A W^{-1}. We find that the perovskite precursor in dimethylformamide solution serve as an excellent stabilizer for the dispersion of carbon nanotubes, which potentially extend the scope of applications of perovskites in solution-processed functional composites. The unprecedented high performances underscore the perovskite/carbon nanotubes hybrids as an emerging class of functional materials in optoelectronic and other applications.

Methylammonium lead trihalide perovskites (MAPbX$_3$, where X is Cl, Br or I) have recently attracted considerable attention as potential next-generation photovoltaic thin-film materials because of their extraordinary physical properties such as adjustable bandgap, large light absorption throughout the UV-Vis region, long carrier diffusion length, as well as cost effectiveness and ease of processing[1-3]. Owing to their superb properties, this class of materials has also been intensively exploited for applications in light-emitting diodes/transistors, photodetectors, lasers, and phototransistors[4-9]. So far, most of these applications are based on polycrystalline perovskite thin films; however, they still suffer from limited carrier mobility due to grain boundaries and structural defects[10,11], which severely circumvent the performance of perovskite-based optoelectronic devices. Perovskite single crystals were demonstrated to exhibit much higher carrier mobilities in the range of 40 – 60 cm^2 V^{-1} s^{-1} (ref. 12, 13), but their bulk form impedes practical device applications.

In advancing optoelectronics, hybrid composites hold great promises in achieving optimal performance because of the synergistic effect of individual building blocks[14-16]. Recently, light-harvesting perovskites have been combined with graphene in hybrid photodetectors[17,18], where

high responsivities have been achieved. Similar to widely studied graphene, single-walled carbon nanotubes (SWNTs) have also been considered as a promising candidate in multifunctional photoelectric devices due to their unique chemical, electrical, optical, thermal, and mechanical properties[19-22]. Particularly, the intrinsic charge carrier mobility in semiconducting SWNTs was estimated to be as high as 10^5 cm^2 V^{-1} s^{-1} (ref. [19]) and SWNTs are effective light absorbers in a wide spectral range[20], which potentially can help enhance the performance of optoelectronic devices employing SWNTs-based hybrid composites. However, SWNTs tend to aggregate into bundles due to strong van der Waals attraction, which is a severe obstacle for its integration with other materials in solution processing[23].

Here, we demonstrate that the perovskite precursor in N, N-dimethylformamide (DMF) solution is an excellent stabilizer for the homogeneous dispersion of SWNTs, enabling the formation of a new type of hybrid composites, which combine the synergetic properties of light-absorbing perovskites with high-mobility SWNTs. Remarkably, introducing SWNTs into the perovskite films leads to an ultrahigh hole mobility of 595.3 cm^2 V^{-1} s^{-1}, which is approximately an order of magnitude higher than those recently reported on perovskite single crystals. Furthermore, the hybrid phototransistors exhibit an excellent photoresponsivity of ~10^4 W A^{-1} and detectivity of ~6.27×10^{14} Jones, which are among the highest values ever reported for organic and inorganic photodetectors. Importantly, the low-cost processing of our hybrid phototransistors potentially facilitates the large-scale developments of practical perovskite-based optoelectronic technologies.

Our design principle of the CH$_3$NH$_3$PbI$_{3-x}$Cl$_x$/SWNTs composites is shown schematically in Fig. 1a. Upon light illumination, the photo-excited holes are expected to effectively transfer from the perovskite matrix to the SWNTs, significantly reducing the charge recombination and enhancing the transport. The SWNTs were characterized using transmission electron microscopy (TEM, Supplementary Fig. 1), and they are approximately 0.5-2 μm in length and 1.4 nm in diameter. The Raman measurement (see Supplementary Fig. 2) further demonstrated the purity of SWNTs. A homogeneous, dark dispersion of SWNTs in DMF solution of CH$_3$NH$_3$I and PbCl$_2$ was prepared, and remarkably, it remained stable for more than 24 h without precipitation; in contrast, the pristine SWNTs quickly precipitated out in DMF solution (see Supplementary Fig. 3). This excellent dispersion is of significant importance for fabricating SWNTs-based devices because SWNTs are known to tend to agglomerate into bundles during preparation due to

3

hydrophobic interactions, which often causes severe inhomogeneity in solution-processed devices and strong performance fluctuation. The excellent dispersion of SWNTs in the precursor of $CH_3NH_3PbI_{3-x}Cl_x$/DMF solution could be attributed to the strong electrostatic interactions among ionic species. The $CH_3NH_3^+$ units in perovskite are preferentially attached to the SWNTs surfaces, endowing the SWNTs with positive charges. As a result, the electrostatic repulsion between SWNTs makes them stably dispersed in the DMF solution.
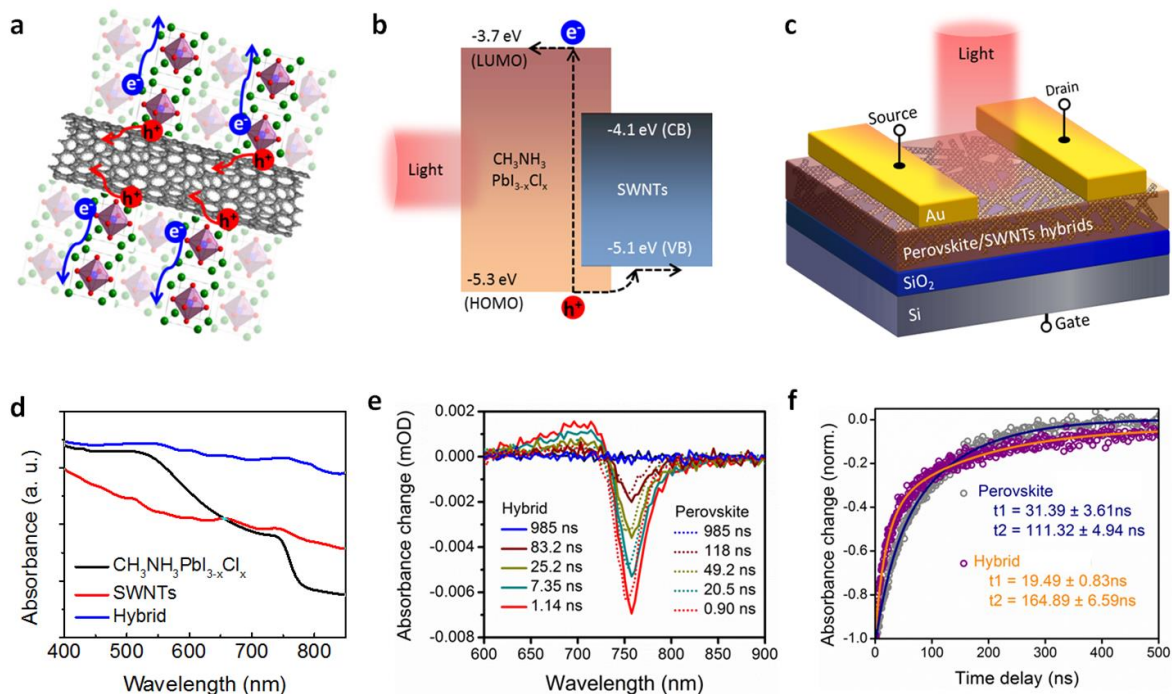

Figure 1 | Design and characterizations of the perovskite/SWNTs hybrids. a, Schematic illustrating the mechanism of fast carrier transport in the perovskite/SWNTs composites. Photo-generated holes are injected into the SWNTs, while electrons are mainly transported by the hybrid perovskite. **b**, Energy-level alignment between perovskite and SWNTs. LUMO, lowest unoccupied molecular orbital; HOMO, highest occupied molecular orbital; CB, conduction band; VB, valence band. **c**, Schematic of the perovskite/SWNTs hybrid phototransistor. **d**, Absorption spectra of the hybrid perovskite/SWNTs, the $CH_3NH_3PbI_{3-x}Cl_x$ and the SWNTs samples. **e**, Transient absorption spectra of the hybrid film measured with light excitation at 480 nm. **f**, Normalized kinetic traces for ground-state bleach of the perovskite and the hybrid films probed at 760 nm and 755 nm, respectively.

The TEM image of the perovskite/SWNTs hybrid film (see Supplementary Fig. 4) further revealed that the crystalline $CH_3NH_3PbI_{3-x}Cl_x$ acted as "glue" for SWNTs, while SWNTs formed a network. The diffraction spots and rings in the selected area electron diffraction (SAED) pattern (inset of Supplementary Fig. 4) belong to the crystalline perovskite and the SWNTs, respectively. Furthermore, the hybrid layer composed of interpenetrating networks of SWNTs in

$CH_3NH_3PbI_{3-x}Cl_x$ matrix exhibited a uniform and continuous surface, as observed in the scanning electron microscopy (SEM, Supplementary Fig. 5a) experiment. In contrast, the reference $CH_3NH_3PbI_{3-x}Cl_x$ film suffered from poor surface coverage and pinholes (Supplementary Fig. 5b). The improved morphology of the hybrid films can be ascribed to the excellent compatibility of $CH_3NH_3PbI_{3-x}Cl_x$ and SWNTs. Finally, the X-ray diffraction (XRD) pattern of the perovskite/SWNTs hybrid film in Supplementary Fig. 6 revealed that $CH_3NH_3PbI_{3-x}Cl_x$ in the channel layer is highly crystalline[3], indicating that the beneficial physical properties of the halide perovskite were largely retained.

It is known that SWNTs might serve as either hole or electron acceptors, which mainly depends on their energy-level alignment with the particular photosensitive materials. In our composites, as shown in Fig. 1b, the valence band (VB) of SWNTs (-5.1 eV)[22] aligns well with the highest occupied molecular orbital (HOMO) level of $CH_3NH_3PbI_{3-x}Cl_x$ (-5.3 eV)[4], which facilitates the injection of photo-excited holes from perovskite into SWNTs. Based on this energy level alignment, Fig. 1b also illuminated the operation mechanism of the composites. Owing to the excellent light absorption property of the perovskite, hole-electron pairs are generated in the hybrid film, and then the holes are injected into SWNTs and transport along the SWNTs under the applied electric field, while the electrons predominantly remain and transport in the perovskite matrix.

As a prototypical demonstration of optoelectronic devices, phototransistors, which have a versatile range of applications in communication, security, lighting, imaging, and data storage technologies[24], were fabricated using the perovskite/SWNTs hybrid as the active channel. The schematic diagram of our phototransistors is illustrated in Fig. 1c. A heavily n-doped Si wafer with a 300-nm SiO_2 surface layer (capacitance C_i: 15 nF cm^{-2}) was employed as the substrate. The perovskites are employed as the light absorber, while SWNTs are expected to facilitate the transportation of photo-excited carriers because of their ultrahigh mobility. In our devices, the thickness of active films is optimized as 400 nm. On one hand, it is known that perovskite films thicker than 300 nm are capable to absorb most of the incident photons. On the other hand, if the film is too thick, gate bias will be screened, degrading the device performance[9].

The wavelength-dependent absorbance of the hybrid perovskite/SWNTs thin film is shown in Fig. 1d. For this measurement, the hybrid film was prepared on a glass substrate using the same

processing parameters as those used in fabricating the phototransistors. The optical absorbance of the pure perovskite and pure SWNTs layers was also characterized as references. The absorption of light in the hybrid film was substantially enhanced in the long-wavelength region as compared to the reference $CH_3NH_3PbI_{3-x}Cl_x$ film. The observed enhancement could be attributed to the strong light absorption of SWNTs[20]. The improvement of light absorption in the hybrid active layer is benefitial to enhance the photosensitivity and detectivity of the hybrid phototransistor. Overall, the strong and broadband light absorption in the ultraviolet and visible-light regimes underscored the hybrid perovskite/SWNTs films as an excellent light absorber, promising for high-performance light-harvesting and optoelectronic applications.

It is well known that the transient absorption spectroscopy can provide direct information regarding the carrier dynamics and excited-state deactivation pathways[25]. As shown in Fig. 1e,f, sharp negative absorption peaks at around 760 nm and broad positive absorption peaks at 600-700 nm in both perovskite and hybrid films are observed. More importantly, the hybrid film exhibits a remarkably strong positive peak in the wide wavelength region from 600 to 700 nm, suggesting intense absorption of the perovskite/SWNTs interfacial excited states. Moreover, the ground-state bleach recovery which mainly reflects the charge recombination is slower in that case of hybrid composites compared to the free $CH_3NH_3PbI_{3-x}Cl_x$, in line with the scenario of hole transfer from the perovskite matrix to the SWNTs. This observation indicates that the charge recombination time constant (τ_{life})[9,14] increases in the phototransistor channel, which will enhance the performance of such hybrid perovskite/SWNTs phototransistors. The steady-state photoluminescence (PL) was also performed to corroborate the scenario of charge transfer at the perovskite/SWNTs interface. A strong quenching of the perovskite PL peak at ~760 nm was observed upon the addition of SWNTs (see Supplementary Fig. 7), further evidencing the excited state interaction at the perovskite/SWNTs interface.

We now turn to the electrical properties of the hybrid phototransistor and propose an operating mechanism. To obtain the transfer characteristics (I_{DS}-V_{GS}) of the hybrid phototransistor in dark (Fig. 2a) and under light illumination (Fig. 2b), we swept the backgate voltage V_{GS} while keeping the source–drain bias V_{DS} across the hybrid channel at fixed values. It should be noted that our device, no matter in the dark or under light, shows clear ambipolar behaviors, i.e., I_{DS} increases with V_{GS} on both polarities. In the absence of light (Fig. 2a), the source-drain current was found to remain below 10 μA in the measurement range of V_{GS}. In contrast, when the device was

illuminated with a white light-emitting diode (LED) at a photoexcitation intensity (E_{light}) of 10 mW cm^{-2}, the channel current reached the level of 10 mA (Fig. 2b), indicating a very high photosensitivity.

The field-effect mobility (μ) and threshold voltage (V_{TH}) can be extracted from the linear regimes of the transfer curves according to[26]:

$$I_{DS} = \frac{W}{L} C_i \mu (V_{GS} - V_{TH}) V_{DS} \tag{1}$$

where W and L are are the width and length of the channel, respectively, and C_i is the gate dielectric capacitance per unit area. By fitting the experimental data to equation (1), the field-effect hole and electron mobilities in the dark were estimated as 0.175 and 0.058 cm^2 V^{-1} s^{-1}, respectively (Fig. 2a). More importantly, in the presence of light illumination, the obtained mobilities of photo-generated holes and electrons are as high as 595.3 and 108.7 cm^2 V^{-1} s^{-1}, respectively (Fig. 2b). The significant increases of hole/electron mobilities on illumination with respect to the dark measurements imply that the photo-induced carriers dominate the channel transport. Furthermore, the ultrahigh room-temperature carrier mobility obtained here is comparable to the values of high-quality crystalline silicon[27], which unambiguously suggest the high potential of the hybrid perovskite/SWNTs films in high-mobility optoelectronic applications.

In line with our previous report[9], for the control devices of perovskite phototransistor without SWNTs, the field-effect hole/electron mobilites are just $1.62 \times 10^{-4}/1.17 \times 10^{-4}$ cm^2 V^{-1} s^{-1} in the dark condition and 1.37/0.87 cm^2 V^{-1} s^{-1} under light illumination (Supplementary Fig. 8). It is obvious that the addition of SWNTs significantly improved the transport property of the phototransistor channel. Even in dark, adding SWNTs increased the channel current from the nA to the μA level. This also indicates that the channel/electrode interfaces are quite transparent in the hybrid devices, allowing high current to flow through. In such devices, the high-mobility SWNTs played a crucial role in enhancing the performance in the hybrid phototransistors. These SWNTs embedded in the perovskite matrix provide fast tracks for carriers to transport with less scattering, which benefits from the good interface and effective charge transfer between perovskites and SWNTs.

As shown in Fig. 2c,d, the typical output characteristics (that is, the dependence of I_{DS} on V_{DS} at different V_{GS}) of the hybrid phototransistor indicate ambipolar behavior, which are consistent

with the transfer characteristics. As expected, both the incident light illumination and the gate voltages can substantially modulate the channel transport. Without the gate voltages, the output curves of the hybrid channel, in both absence and presence of light, appear almost symmetric. However, with a high negative V_{GS}, the channel transport exhibits the characteristics of a diode with good rectification ratios, while a high positive V_{GS} reverses the rectification of the diode. Furthermore, these data indicate that p-type conduction is slightly favored, i.e., higher current is consistently achieved with negative gate bias.
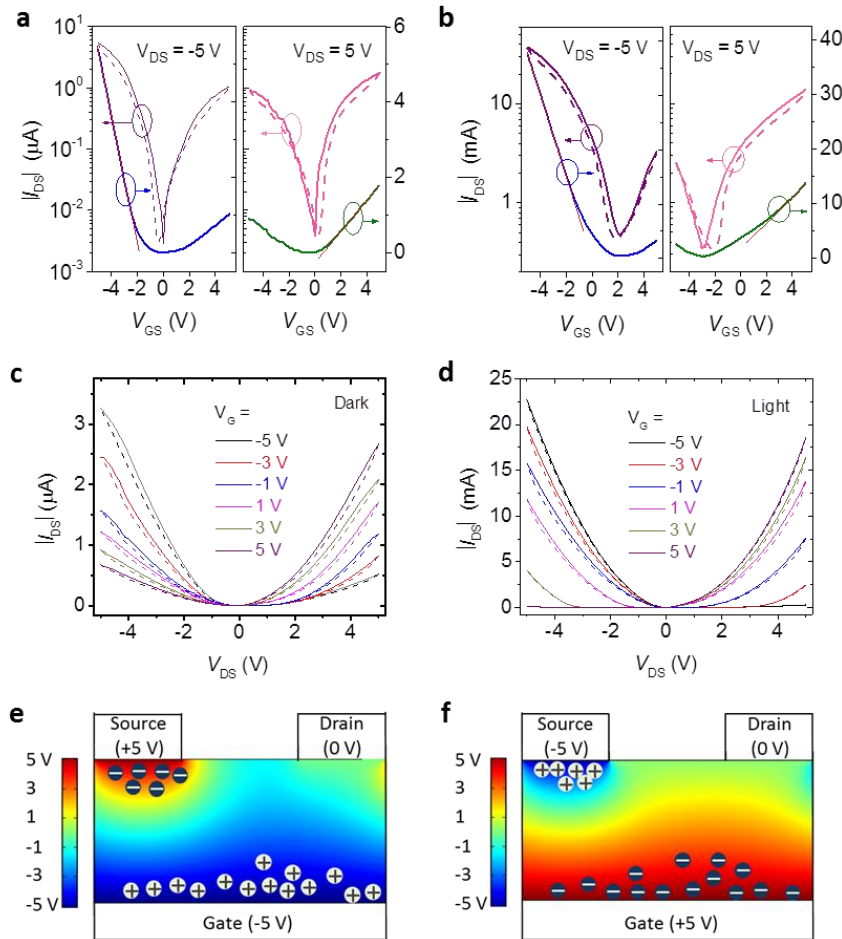
Figure 2 | Ambipolar transport of the hybrid perovskite/SWNTs phototransistor. a,b, Transfer characteristics (I_{DS}-V_{GS}) of the hybrid perovskite/SWNTs phototransistor operating in the absence and presence of light, respectively. **c,d**, Output characteristics (I_{DS}-V_{DS}) of the hybrid phototransistor operating in dark and under light illumination, respectively. **e,f**, Simulation of the electric field distribution in the hybrid channel at two typical bias configurations. The accumulated ions in the hybrids near the electrodes induced strongly localized p- and n- doped areas.

It is a consensus that there are high-density charged defects in perovskite due to their low formation energies, including both positively charged defects (such as I vacancies) and

8

negatively charged ones (such as Pb and CH_3NH_3 vacancies)[28]. It was also recently reported that an electric field could cause the drift of these charged ions toward the electrodes[29]. Indeed, both the transfer curves and the output curves exhibit small but notable hysteresis effects (Fig. 2a-d), consisting with the screening effects arising from the field-induced drift of charged defects[5,9,29]. Accordingly, we propose that in the phototransistor operation, the distribution of the ionic defects and the perovskite/electrode interfaces could be significantly modulated by the distribution of electric field in the channel. The simulation results of the potential distributions in the hybrid channel are illustrated in Fig. 2e,f and Supplementary Fig. 9. At V_{DS} = +5 V and V_{GS} = -5 V (Fig. 2e), the largest potential difference occurs between the gate and source electrodes, and negative ions drift toward the source electrode, forming a strongly localized n-doped area, which significantly enhances the Schottkey barrier at the channel/electrode interface and reduces the channel current. When V_{DS} scans to -5 V, less ionic drift occurs, which explain the rectifying channel transport. On the other hand, when the gate bias is reversed, i.e., V_{GS} = +5 V, as shown in Fig. 2f, the most significant drift of ions should occur mainly at V_{DS} = -5 V, which leads to reversed rectification of the channel in reference to the case of negative V_{GS}. As expected, without any gate bias, the channel transport showed symmetric behavior without any current rectification (Supplementary Fig. 10).

Photoresponsivity (R), indicating how efficiently the optoelectronic device responds to an optical signal, is an important figure-of-merit for evaluating the performance of phototransistors. It is given by $R = (I_{light}-I_{dark})/E_{light}$, where I_{light} and I_{dark} are the channel currents under light illumination and in dark, respectively. R as a function of V_{GS} measured on our phototransistors is shown in Fig. 3a, and the maximum R is approximately 1.17×10^4 A W^{-1}. Note that this R value is among the largest values reported for phototransistors[7-9,30]. In contrast, the maximum R of a $CH_3NH_3PbI_{3-x}Cl_x$-based phototransistor is about 13 A W^{-1} (see Supplementary Fig. 11a). The much-enhanced R of our hybrid phototransistor indicates the synergy between the halide perovskite and the SWNTs in the hybrid channel.

In addition to photoresponsivity, specific detectivity D^* (measured in units of Jones, Jones = cm Hz$^{1/2}$ W^{-1}) is another critical parameter for evaluating the performance of photodetectors, which characterizes the capability of the devices to detect the incident light signal. The noise current is the main factor to limit the specific detectivity of a photodetector, and the total noise current of our phototransistor was directly measured with a lock-in amplifier at various

9

frequencies. As shown in Fig. 3b, the measured noise current was dominated by the shot noise, and accordingly, the specific detectivity of a photodetector is given by[7]

$$D^* = \frac{(Af)^{1/2}}{(i_n / R)} \qquad (2)$$

where A, f and i_n are the effective area of the device, the electrical bandwidth and the noise current, respectively. In our case, since the shot noise from the dark current is the major contribution to the noise limiting the detectivity, the detectivity can be simplified as

$$D^* = \frac{R}{(2qI_{dark} / A)^{1/2}} \qquad (3)$$

where q is the absolute value of electron charge (1.602×10^{-19} Coulombs) and I_{dark}/A is the dark current density. The detectivity, together with the photoresponsivity, of our hybrid phototransistor as a function of wavelength is plotted in Fig. 3c. At an illumination light intensity of 10 mW cm^{-2}, the maximum D^* of 6.27×10^{14} Jones at about 400 nm was obtained from the hybrid device, whereas the phototransistor based on the pristine perovskite showed a much lower D^* of 4.0×10^{12} Jones (see Supplementary Fig. 11b). We note here that the obtained D^* value is comparable to the highest values ever reported for both organic and inorganic photodetectors[9,16,17,30]. Such high D^* of the hybrid phototransistor in combination with the simple device architecture enables the detection of very weak light signal, promising for high-sensitivity photodetector applications.

As the most significant finding, ultrahigh mobility was achieved by adding the SWNTs into the perovskite films. In order to examine the role of SWNTs, we investigated the performance of phototransistors using hybrid films with varied SWNTs concentrations. As shown in Fig. 3d, the highest mobility and the optimal device performance were obtained at the SWNT concentration of 1 wt. %. We should note that the hole mobility of nearly 600 cm^2 V^{-1} s^{-1} is the highest among the values reported for perovskite-based materials, even much higher than that of the perovskite single crystals[12,13]. In our hybrid films, SWNTs play the important roles of interacting with the perovskite and transporting charges, significantly improving the overall mobility. However, at the highest SWNT concentration (3 wt. %), the hybrid phototransistor showed high conductance but weak p-type field effect (Supplementary Fig. 12), indicating that the SWNTs started to form a percolation network which dominated the charge transport. Since photocurrent is proportional

to mobility, the optimal photoresponsivity and detectivity of the phototransistors were also achieved at the SWNTs concentration of 1 wt.% (Fig. 3d).
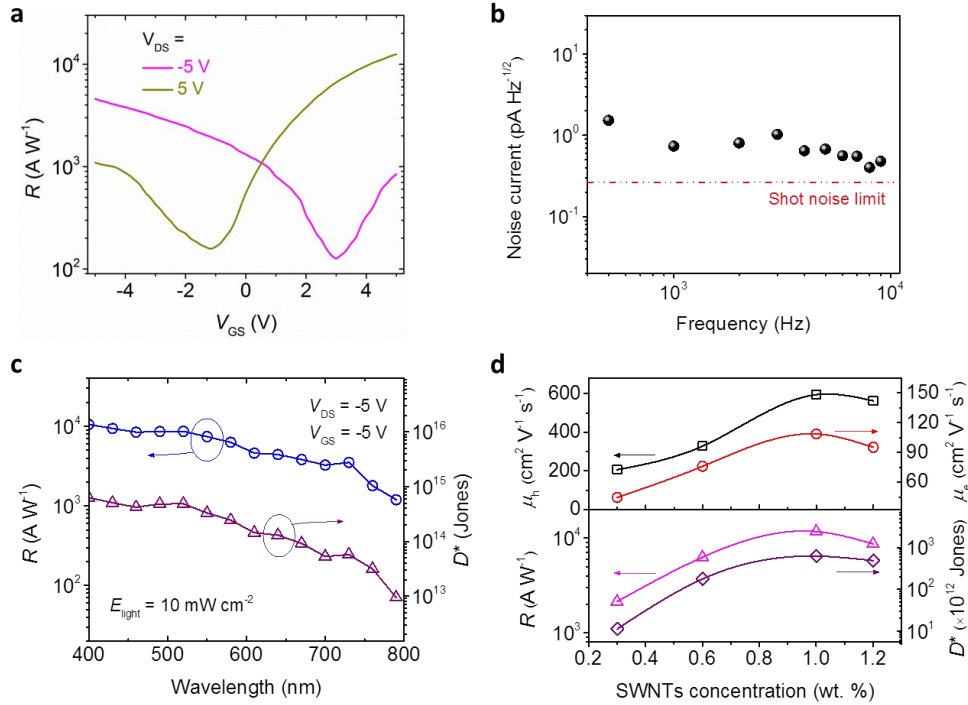

Figure 3 | Performance of the hybrid perovskite/SWNTs phototransistor. a, Responsivity (R) of the phototransistor as a function of back-gate voltage. The maximum responsivity reaches approximately 1.17×10^{4} A W^{-1}. **b**, Noise current of the hybrid phototransistor. Measured noise current of the hybrid perovskite-SWNTs phototransistor at different frequencies. The calculated shot noise limit is also plotted for comparison. **c**, Responsivity (R) and Detectivity (D^*) of the hybrid phototransistor measured at different wavelengths with the light intensity of 10 mW cm^{-2}. **d**, Effect of the SWNTs concentration on the performance of the hybrid perovskite-SWNTs phototransistor. μ_h, μ_e, R and D^* denote hole mobility, electron mobility, responsivity and detectivity, respectively.

Another important parameter of optoelectronic devices is their response speed. The temporal response of our hybrid phototransistor was characterized using chopper-generated light pulses. The optical pulses had the time interval of 1.0 s and an intensity of 10 mW cm^{-2}, and the device was measured under the biases of V_{DS} = -3 V and V_{GS} = -3 V. As shown in Fig. 4a, the dynamic photoresponse of the hybrid phototransistor is stable and reproducible, indicating that the device can function as a good light switch. The temporal photocurrent response of the hybrid phototransistor is presented in Fig. 4b. The switching times for the rise (output signal changing from 0 to 90% of the peak output value) and the decay (I_{DS} decreasing from peak value to 10%) of the photocurrent are about 738 μs and 912 μs, respectively, which can also be taken as the

carrier lifetime τ_{life}. It is noted that the response speed of our hybrid phototransistor is faster than most of the organic, quantum dot and hybrid photodetectors (typically on the order of milliseconds)[14-18,30,31], which arise from the good carrier transport in the hybrid films. The photoconductive gain (G) is the ratio between τ_{life} and the transit time (τ_{tran}, which is the time during which holes sweep through the SWNTs to the electrodes), and given by[9,14,16,22]

$$G = \frac{\tau_{\text{life}}}{\tau_{\text{tran}}} = \frac{\tau_{\text{life}}}{L^2 / \mu \cdot V_{\text{DS}}} \tag{4}$$

Based on the measured carrier recombination time and the carrier mobility, the gain of our hybrid devices was estimated as approximately 8000, which further underscores the hybrid perovskite/SWNTs films as a promising material candidate for photoelectronic applications.
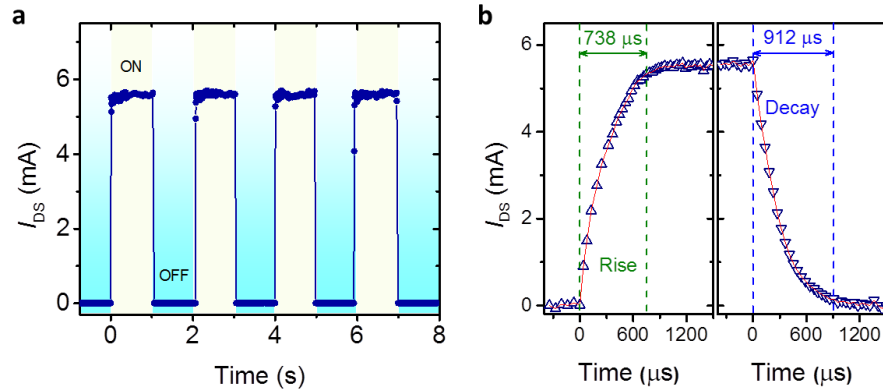
Figure 4 | Photocurrent response of the hybrid perovskite/SWNTs phototransistor. a, Temporal Photocurrent responsive characteristic of the hybrid perovskite/SWCNTs phototransistor measured at V_{GS} = -3 V and V_{DS} = -3 V, respectively. **b**, Temporal photocurrent response, indicating a rise time of 738 μs and a decay time of 912 μs.

In summary, we demonstrated a novel type of hybrid thin film materials combining light-absorbing perovskite and carrier-transporting SWNTs. Owing to the excellent compatibility of the perovskite and the SWNTs, high-quality hybrid films were achieved from the stable mixtures, and the physical properties of both constituents were synergistically retained. As a prototypical device, high-performance ambipolar phototransistors based on the solution-processed perovskite/SWNTs hybrid films were fabricated. In the hybrid phototransistor channels, SWNTs provide fast tracks for carrier transport, significantly improving the field effect mobility of photo-carriers. By varying the SWNTs weight concentration, we found that the field effect mobility of photo-generated holes could reach as high as 595.3 cm^2 V^{-1} s^{-1}. The phototransistors

combining perovskite and SWNTs resulted in ultrahigh specific detectivity of 6.27×10^{14} Jones and responsivity of 1.17×10^{4} A W^{-1}. From a general perspective, these perovskite/SWNTs composite films open up a new door towards developing novel optoelectronic devices, and the strategy may help advance other hybrid-based technologies.

Methods

Perovskite/SWNTs hybrid solution preparation. Semiconducting SWNTs (Sigma-Aldrich, > 90 wt %) were purified and partially oxidized via refluxing in 3M HNO$_3$ for 12 h. Then, the SWNTs were separated by ultracentrifugation, washed with excess of water several times and freeze-dried. Methylammonium iodide (MAI) and lead(II) chloride (PbCl$_2$, Sigma-Aldrich, 98%) were dissolved in DMF (Sigma-Aldrich, 99.8%) with a molar ratio 3:1 to form the perovskite precursor solution. To form the hybrid solution, the purified SWNTs was mixed into the perovskite solution upon sonication for 2 h., with the SWNTs/perovskite weight concentration ranging from 0 and 3%. We note that the precursor solution must be stored in glove box and used quickly after mixing to avoid degradation.

Device fabrication. Si/SiO$_2$ (300 nm) substrates were cleaned by sonication in acetone, ethanol and deionized water, respectively. After drying in flowing nitrogen, we treated the substrates with oxygen plasma. The hybrid solution was spin-coated on substrates at 2000 rpm for 20 seconds and annealed at 100 °C for 60 minutes in a glove box. For comparison, pristine perovskite films were prepared in the same way without SWCTs. Ti/Au (5 nm/80 nm) source (S) and drain (D) electrodes were deposited via thermal evaporation through a shadow mask, defining phototransistor channels with length of 50 µm and width of 1000 µm. Finally, the fabricated devices were annealed to reduce the charge traps and to improve the contacts between the active layer and the S/D electrodes.

Measurements. XRD was performed on a Bruker D8-Advance diffractometer using Cu Kα radiation (λ = 1.5406 Å). The surface morphology of the films was measured using SEM (FEI Nova Nano 630). TEM experiments were carried out using a Titan ST instrument operated at 300 kV. The absorption and steady-state PL were recorded using Cary 6000i spectrophotometer with an Edinburgh Instrument spectrofluorometer. Ultrafast Systems Helios UV-NIR femtosecond transient absorption spectroscopy system was also used to characterize the samples. Transport measurements were conducted using a Signotone Micromanipulator S-1160 probe station equipped with a LED and Keithley 4200 SCS. Noise current was measured with a lock-in amplifier SR830.

References

1. Xing, G. *et al*. Long-range balanced electron- and hole-transport lengths in organic-inorganic CH$_3$NH$_3$PbI$_3$. *Science* **342,** 344–347 (2013).

2. Stranks, S. D. *et al*. Electron-hole diffusion lengths exceeding 1 micrometer in an organometal trihalide perovskite absorber. *Science* **342,** 341–344 (2013).

3. Stranks, S. D. & Snaith, H. J. Metal-halide perovskites for photovoltaic and light-emitting devices. *Nature Nanotech.* **10,** 391-402 (2015).

4. Tan, Z.-K. *et al*. Bright light-emitting diodes based on organometal halide perovskite. *Nature Nanotech.* **9,** 687–692 (2014).

5. Chin, X. Y., Cortecchia, D., Yin, J., Bruno, A. & Soci, C. Lead iodide perovskite light-emitting field-effect transistor. *Nature Commun*. **6,** 7383 (2015).

6. Xing, G. *et al*. Low-temperature solution-processed wavelength-tunable perovskites for lasing. *Nature Mater.* **13,** 476–480 (2014).

7. Dou, L. *et al*. Solution-processed hybrid perovskite photodetectors with high detectivity. *Nature Commun.* **5,** 5404 (2014).

8. Dong, R. *et al*. High-gain and low-driving-voltage photodetectors based on organolead triiodide perovskites. *Adv. Mater.* **27,** 1912–1918 (2015).

9. Li, F., Ma, C., Wang, H., Hu, W., Yu, W., Sheikh, A. D. & Wu, T. Ambipolar solution-processed hybrid perovskite phototransistors. *Nature Commun*. **6,** 8238 (2015).

10. Gratzel, M. The light and shade of perovskite solar cells. *Nature Mater.* **13,** 838-842 (2014).

11. Shao, Y., Xiao, Z., Bi, C., Yuan, Y. & Huang, J. Origin and elimination of photocurrent hysteresis by fullerene passivation in CH$_3$NH$_3$PbI$_3$ planar heterojunction solar cells. *Nature Commun.* **5,** 5784 (2014).

12. Shi, D. *et al.* Low trap-state density and long carrier diffusion in organolead trihalide perovskite single crystals. *Science* **347,** 519-522 (2015).

13. Dong, Q., Fang, Y., Shao, Y., Mulligan P., Qiu, J., Cao, L., Huang, J. Electron-hole diffusion lengths > 175 mm in solution-grown CH3NH3PbI3 single crystals. *Science* **347**, 967-970 (2015).

14. Konstantatos, G. *et al*. Hybrid graphene–quantum dot phototransistors with ultrahigh gain. *Nature Nanotech.* **7,** 363–368 (2012).

15. Roy, K. *et al.* Graphene-MoS$_2$ hybrid structures for multifunctional photoresponsive memory devices. *Nat. Nanotech.* **8,** 826-830 (2013).

16. Koppens, F. H. L. *et al*. Photodetectors based on graphene, other two dimensional materials and hybrid systems. *Nature Nanotech*. **9,** 780–793 (2014).

17. Lee, Y. *et al*. High-performance perovskite–graphene hybrid photodetector. *Adv. Mater.* **27,** 41–46 (2015).

18. Spina, M. *et al*. Microengineered CH$_3$NH$_3$PbI$_3$ nanowire/graphene phototransistor for low-intensity light detection at room temperature. *Small* **11,** 4824–4828 (2015).

19. Yu, M. F., Files, B. S., Arepalli, S. & Ruoff, R. S. Tensile loading of ropes of single wall carbon nanotubes and their mechanical properties. *Phys. Rev. Lett*. **84,** 5552−5555 (2000).

20. Avouris, P., Freitag, M. & Perebeinos, V. Carbon-nanotube photonics and optoelectronics. *Nature Photon.* **2,** 341-350 (2008).

21. Liu, X. *et al*. Rational design of amorphous indium zinc oxide/carbon nanotube hybrid film for unique performance transistors. *Nano Lett*. **12,** 3596−3601 (2012).

22. Park, S. *et al*. Significant enhancement of infrared photodetector sensitivity using a semiconducting single-walled carbon nanotube/C_{60} phototransistor. *Adv. Mater.* **27,** 759-765 (2015).

23. Bandyopadhyaya, R. *et al.* Stabilization of individual carbon nanotubes in aqueous solutions. *Nano Lett.* **2,** 25-28 (2002).

24. Liu, J.-M. *Photonic Devices* (Cambridge University Press, Cambridge, UK 2009).

25. Mohammed, O. F. *et al*. Excited-state intramolecular hydrogen transfer (ESIHT) of 1,8-dihydroxy-9,10-anthraquinone (DHAQ) characterized by ultrafast electronic and vibrational spectroscopy and computational modeling. *J. Phys. Chem. A* **118,** 3090−3099 (2014).

26. Schroder, D. K. *Semiconductor Material and Device Characterization* (Wiley, 2006).

27. Prince, N. B. Drift mobilities in semiconductors. II. Silicon. *Phys. Rev.* **93,** 1204-1206 (1954).

28. Kim, J., Lee, S.-H., Lee, J. H. & Hong, K.-H. The role of intrinsic defects in methylammonium lead iodide perovskite. *J. Phys. Chem. Lett*. **5,** 1312-1317 (2014).

29. Xiao, Z. *et al*. Giant switchable photovoltaic effect in organometal trihalide perovskite devices. *Nature Mater.* **14,** 193-198 (2015).

30. Baeg, K.-J., Binda, M., Natali, D., Caironi, M. & Noh, Y.-Y. Organic light detectors: photodiodes and phototransistors. *Adv. Mater*. **25,** 4267–4295 (2013).

31. Konstantatos, G. *et al*. Ultrasensitive solution-cast quantum dot photodetectors. *Nature* **442,** 180–183 (2006).

Acknowledgements

Supplementary Information

Achieving ultrahigh carrier mobility and photo-responsivity in solution-processed perovskite/carbon nanotube phototransistors

Hong Wang[1][†], Feng Li[1][†], Dominik Kufer[2], Weili Yu[1], Erkki Alarousu[3], Chun Ma[1], Yangyang Li[1], Zhixiong Liu[1], Changxu Liu[4], Nini Wei[5], Yin Chen[3], Fei Wang[6], Lang Chen[6], Omar F. Mohammed[3], Andrea Fratalocchi[4], Gerasimos Konstantatos[2], Tom Wu[1]*

[1]Materials Science and Engineering, King Abdullah University of Science and Technology, Thuwal 23955-6900, Kingdom of Saudi Arabia.

[2]ICFO- Institut de Ciencies Fotoniques, Mediterranean Technology Park, 08860 Castelldefels, Barcelona, Spain.

[3]Solar and Photovoltaics Engineering Research Center, King Abdullah University of Science and Technology, Thuwal 23955-6900, Kingdom of Saudi Arabia.

[4]PRIMALIGHT, Faculty of Electrical Engineering, Applied Mathematics and Computational Science, King Abdullah University of Science and Technology, Thuwal 23955-6900, Saudi Arabia.

[5]Core lab, King Abdullah University of Science and Technology, Thuwal 23955-6900, Kingdom of Saudi Arabia.

[6]Department of Electronic and Electrical Engineering, South University of Science and Technology of China, Shenzhen 518055, P.R. China.

[†]These authors contributed equally to this work.

*e-mail: tao.wu@kaust.edu.sa

Supplementary Figure 1 | HRTEM image of a SWNT. High-resolution transmission electron microscopy (HRTEM) image of a SWNT used to fabricate the perovskite/SWNTs hybrids. The diameter of SWNT is about 1.4 nm.
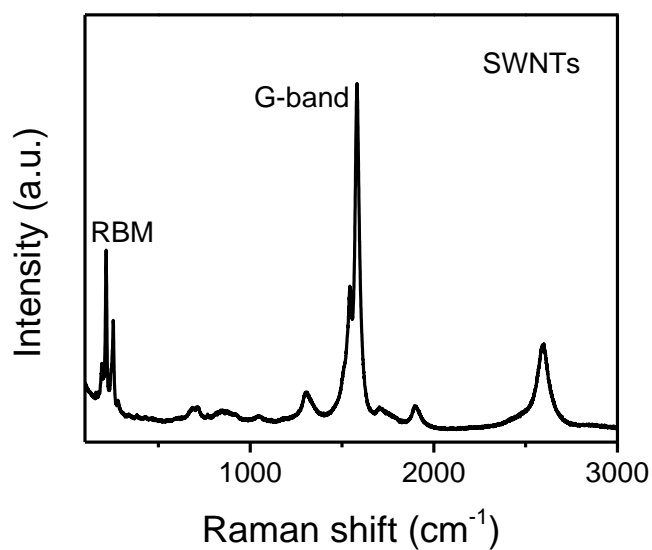

Supplementary Figure 2 | Raman spectrum of SWNTs. The Raman spectrum of SWNTs used to fabricate perovskite/SWNTs hybrids.

Supplementary Figure 3 | Digital photographs of samples. Digital photographs of (I) the $CH_3NH_3PbI_{3-x}Cl_x$/SWNTs precursor and (II) SWNTs in N, N-dimethylformamide (DMF) solutions taken 24 h after preparation. A homogeneous, dark dispersion of SWNTs in DMF solution of CH_3NH_3I and $PbCl_2$ was prepared, and remarkably, it remained stable for more than 24 h without precipitation, while the pristine SWNTs quickly precipitated out in DMF solution.
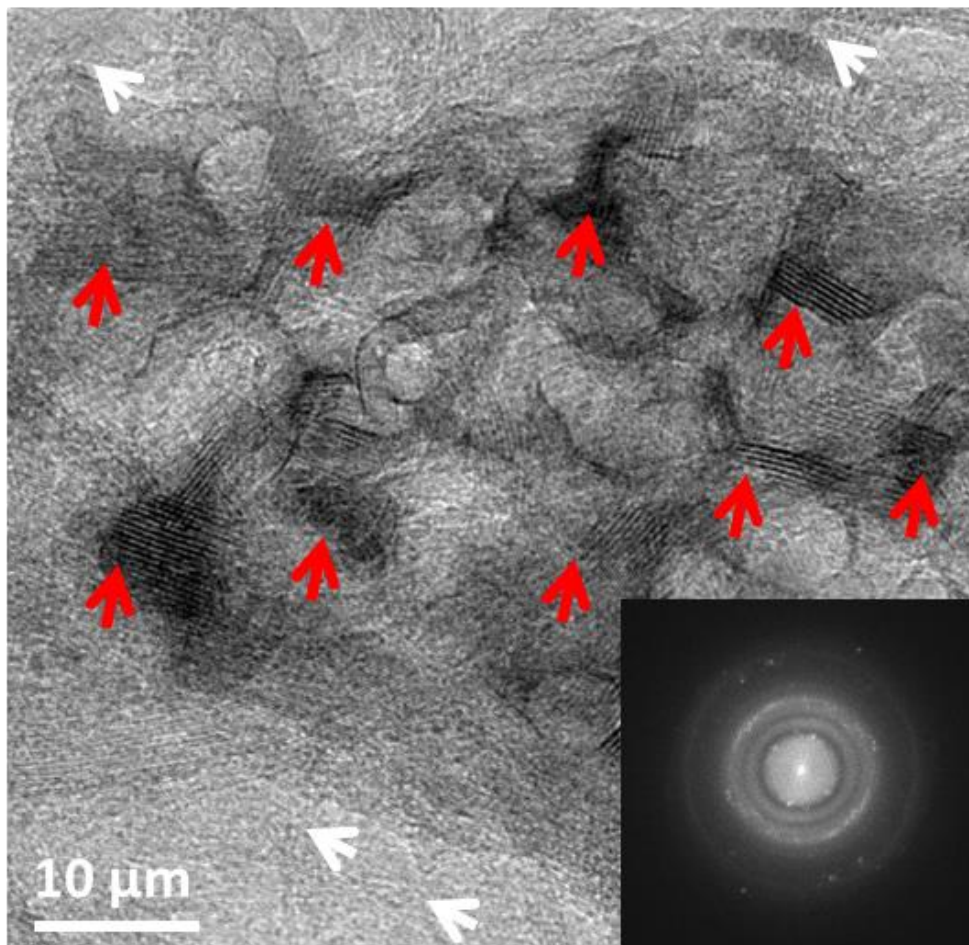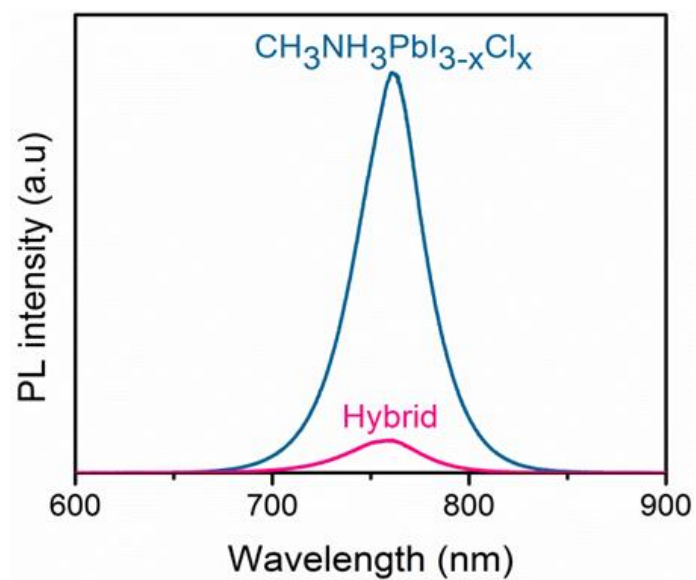
Supplementary Figure 4 | TEM image of the hybrid film. Transmission electron microscopy (TEM) image of the hybrid perovskite/SWNTs film, inset shows the selected area electron diffraction (SAED) pattern. Red and white arrows indicate the crystalline $CH_3NH_3PbI_{3-x}Cl_x$ and SWNTs, respectively. Symmetric diffraction spots and continuous diffraction rings displayed in the SAED pattern belong to crystalline perovskite and SWNTs, respectively.
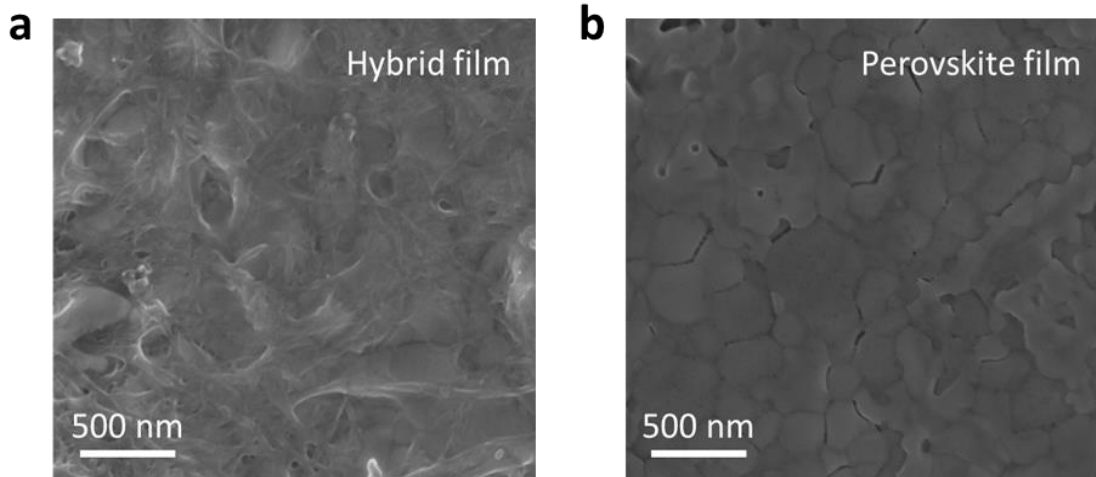
Supplementary Figure 5 | SEM images of the films. a, Scanning electron microscopy (SEM) image of the perovskite/SWNTs film on Si/SiO$_2$ substrate. The hybrid thin film appears smooth and uniform surface morphology. Some SWNTs replace perovskites in the hybrid thin film, and the superior tracks are used to achieve carrier transport with less scatter. **b**, SEM image of a pristine perovskite film on Si/SiO$_2$ substrate. The pristine perovskite film suffers from poor surface coverage and pinholes.
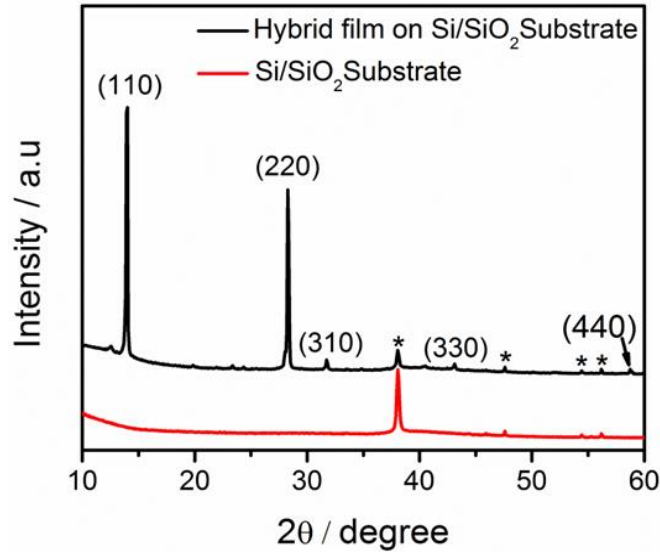
Supplementary Figure 6 | XRD pattern of the films. X-ray diffraction (XRD) spectra of the hybrid perovskite/SWNTs film on Si/SiO_2 substrate (black line) and the sole Si/SiO_2 substrate (red line), respectively. The peaks marked with * belong to the Si/SiO_2 substrate. The main diffraction peaks at 14.02°, 28.35°, 37.74°, 43.16° and 58.78° can be assigned to <110>, <220>, <310>, <330>, <440> planes of the perovskite, respectively, which the perovskite $CH_3NH_3PbI_{3-x}Cl_x$ composited to hybrid thin film possess the expected orthorhombic crystal structure with high crystallinity.

Supplementary Figure 7 | PL spectra. Steady-state photoluminescence (PL) spectra of the hybrid perovskite/SWNTs and the pristine perovskite films. A strong quenching of the perovskite PL peak at ~760 nm was observed upon the addition of SWNTs.
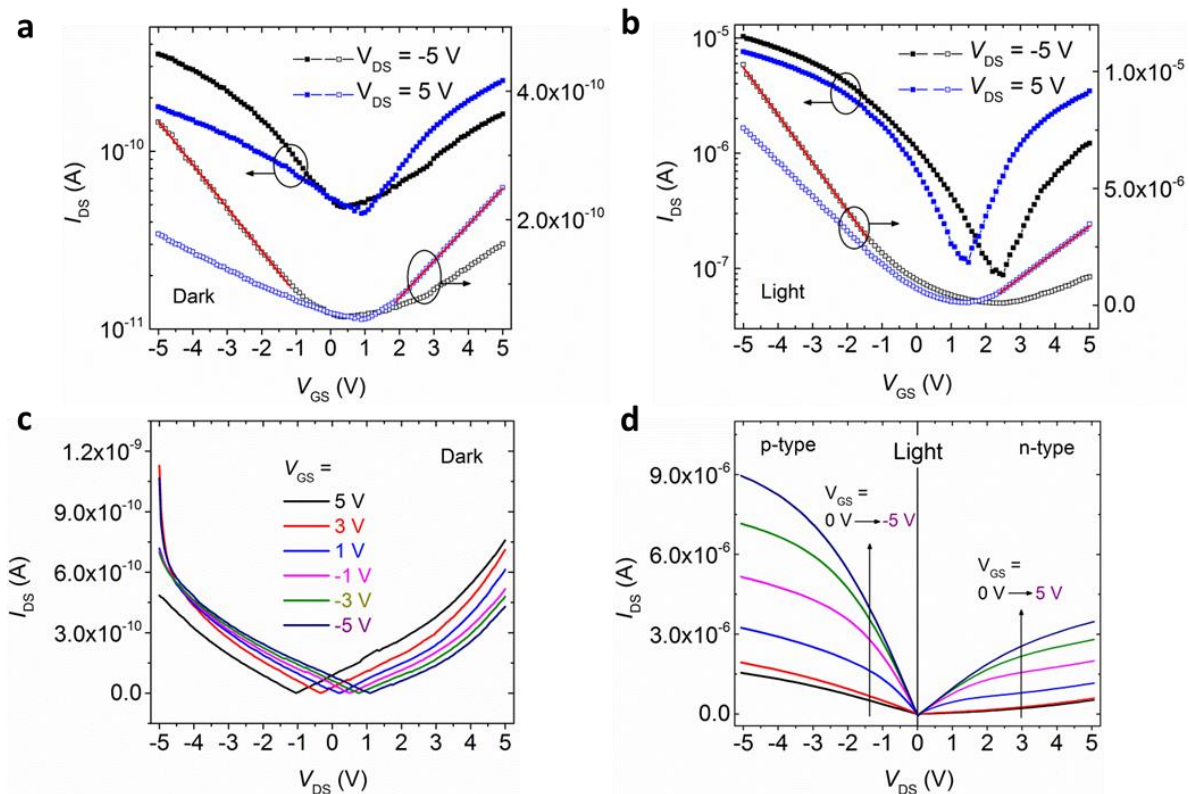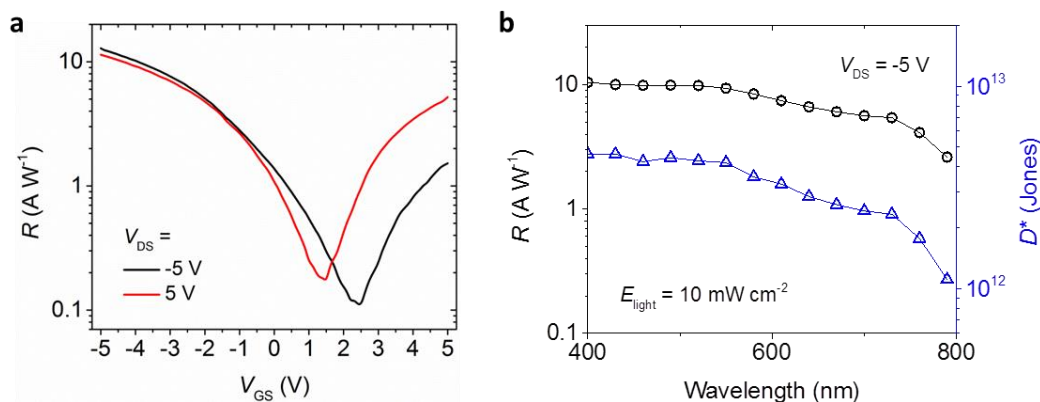
Supplementary Figure 8 | Performance of a control device employed the pure perovskites in the phototransistor channel. a,b, Transfer characteristics of the perovskite-based phototransistor in the dark and under light illumination, respectively. The field-effect hole/electron mobilites, calculated from the transconductance using $I_{DS} = \dfrac{W}{L} C_i \mu (V_{GS} - V_{TH}) V_{DS}$ in the linear regime, are just $1.62 \times 10^{-4}/1.17 \times 10^{-4}$ cm^2 V^{-1} s^{-1} in the dark condition and $1.37/0.87$ cm^2 V^{-1} s^{-1} under light illumination, respectively. **c,d**, Output characteristic of the perovskite phototransistor in dark and under light illumination, respectively.
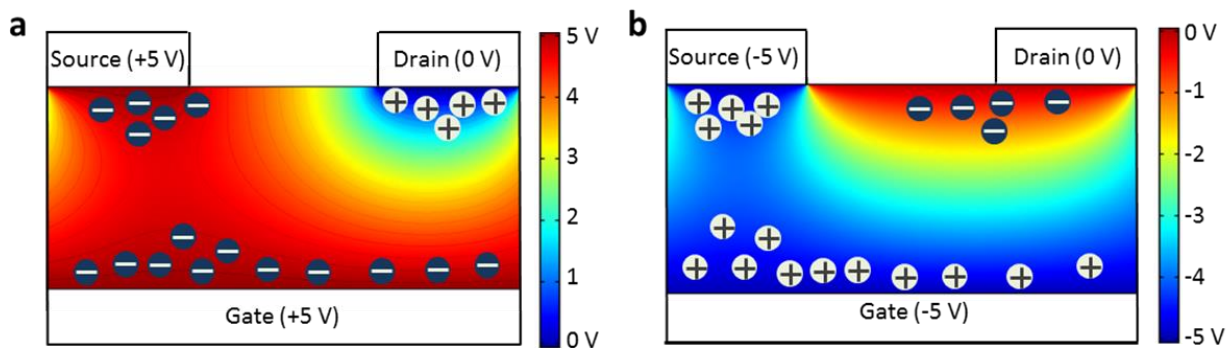
Supplementary Figure 9 | Simulation of the electric field distribution in the hybrid channel at other two typical bias configurations. a, Simulation of the electric field distribution in the hybrid channel when using positive source voltage of +5 V and positive gate voltage of +5 V. **b,** Simulation of the electric field distribution in the hybrid channel when using negative source voltage of -5 V and negative gate voltage of -5 V. The accumulated ions in the hybrids near the electrodes induced strongly localized p- and n- doped areas.
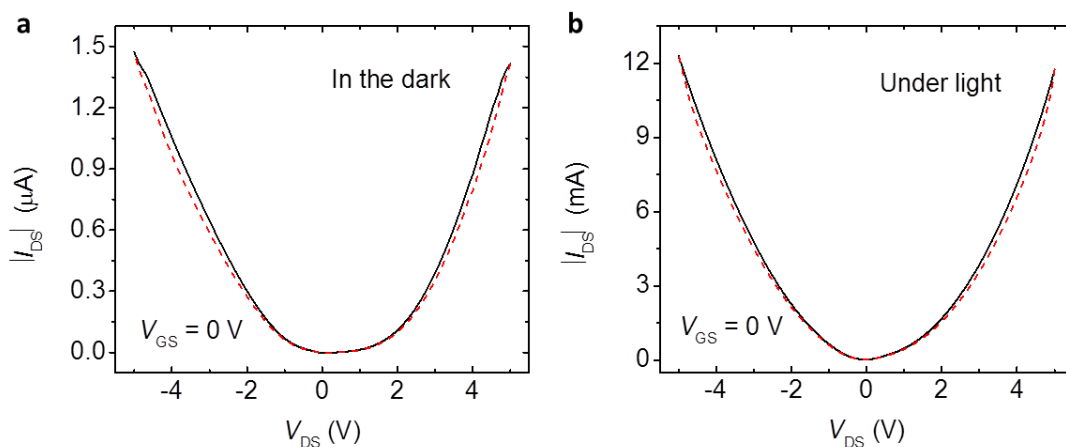
Supplementary Figure 10 | *I-V* curves for the device without the gate bias. The dependence of I_{DS} on V_{DS} for the hybrid phototransistor at V_{GS} = 0 V, measured in the dark and under light illumination, showing symmetric behavior without any current rectification.

Supplementary Figure 11 | Performance of the perovskite phototransistor. a, Responsivity (*R*) of the perovskite-based phototransistor operating at V_{DS} = -5 V and V_{DS} = 5 V, respectively. **b**, Responsivity (*R*) and specific detectivity (*D**) of the perovskite phototransistor at different wavelengths with the light intensity of 10 mW cm^{-2}.
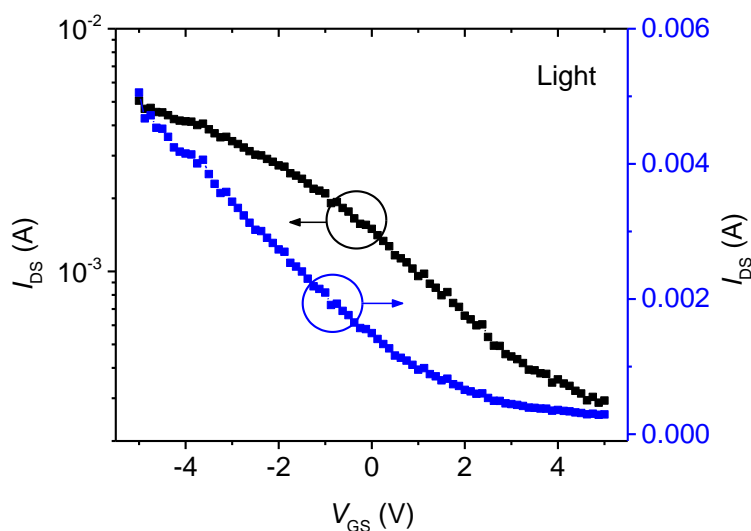
Supplementary Figure 12 | Transfer characteristics of a hybrid phototransistor with the SWNTs concentration of 3 wt. %. Transfer characteristics of a hybrid device with the higher SWNTs concentration (3 wt. %) were measured, the hybrid film presents high conductance but a weak p-type field effect, indicating the SWNTs are starting to make a fully percolation network to dominate the charge transport.